

Observation of $B^0 \rightarrow \chi_{c0} K^{*0}$ and evidence for $B^+ \rightarrow \chi_{c0} K^{*+}$

B. Aubert,¹ M. Bona,¹ Y. Karyotakis,¹ J. P. Lees,¹ V. Poireau,¹ E. Principe,¹ X. Prudent,¹ V. Tisserand,¹ J. Garra Tico,² E. Grauges,² L. Lopez,^{3a,3b} A. Palano,^{3a,3b} M. Pappagallo,^{3a,3b} G. Eigen,⁴ B. Stugu,⁴ L. Sun,⁴ G. S. Abrams,⁵ M. Battaglia,⁵ D. N. Brown,⁵ R. N. Cahn,⁵ R. G. Jacobsen,⁵ L. T. Kerth,⁵ Yu. G. Kolomensky,⁵ G. Lynch,⁵ I. L. Osipenko,⁵ M. T. Ronan,^{5,*} K. Tackmann,⁵ T. Tanabe,⁵ C. M. Hawkes,⁶ N. Soni,⁶ A. T. Watson,⁶ H. Koch,⁷ T. Schroeder,⁷ D. Walker,⁸ D. J. Asgeirsson,⁹ B. G. Fulsom,⁹ C. Hearty,⁹ T. S. Mattison,⁹ J. A. McKenna,⁹ M. Barrett,¹⁰ A. Khan,¹⁰ V. E. Blinov,¹¹ A. D. Bukin,¹¹ A. R. Buzykaev,¹¹ V. P. Druzhinin,¹¹ V. B. Golubev,¹¹ A. P. Onuchin,¹¹ S. I. Serednyakov,¹¹ Yu. I. Skovpen,¹¹ E. P. Solodov,¹¹ K. Yu. Todyshev,¹¹ M. Bondioli,¹² S. Curry,¹² I. Eschrich,¹² D. Kirkby,¹² A. J. Lankford,¹² P. Lund,¹² M. Mandelkern,¹² E. C. Martin,¹² D. P. Stoker,¹² S. Abachi,¹³ C. Buchanan,¹³ J. W. Gary,¹⁴ F. Liu,¹⁴ O. Long,¹⁴ B. C. Shen,^{14,*} G. M. Vitug,¹⁴ Z. Yasin,¹⁴ L. Zhang,¹⁴ V. Sharma,¹⁵ C. Campagnari,¹⁶ T. M. Hong,¹⁶ D. Kovalskyi,¹⁶ M. A. Mazur,¹⁶ J. D. Richman,¹⁶ T. W. Beck,¹⁷ A. M. Eisner,¹⁷ C. J. Flacco,¹⁷ C. A. Heusch,¹⁷ J. Kroseberg,¹⁷ W. S. Lockman,¹⁷ A. J. Martinez,¹⁷ T. Schalk,¹⁷ B. A. Schumm,¹⁷ A. Seiden,¹⁷ M. G. Wilson,¹⁷ L. O. Winstrom,¹⁷ C. H. Cheng,¹⁸ D. A. Doll,¹⁸ B. Echenard,¹⁸ F. Fang,¹⁸ D. G. Hitlin,¹⁸ I. Narsky,¹⁸ T. Piatenko,¹⁸ F. C. Porter,¹⁸ R. Andreassen,¹⁹ G. Mancinelli,¹⁹ B. T. Meadows,¹⁹ K. Mishra,¹⁹ M. D. Sokoloff,¹⁹ P. C. Bloom,²⁰ W. T. Ford,²⁰ A. Gaz,²⁰ J. F. Hirschauer,²⁰ M. Nagel,²⁰ U. Nauenberg,²⁰ J. G. Smith,²⁰ K. A. Ulmer,²⁰ S. R. Wagner,²⁰ R. Ayad,^{21,+} A. Soffer,^{21,*} W. H. Toki,²¹ R. J. Wilson,²¹ D. D. Altenburg,²² E. Feltresi,²² A. Hauke,²² H. Jasper,²² M. Karbach,²² J. Merkel,²² A. Petzold,²² B. Spaan,²² K. Wacker,²² M. J. Kobel,²³ W. F. Mader,²³ R. Nogowski,²³ K. R. Schubert,²³ R. Schwierz,²³ A. Volk,²³ D. Bernard,²⁴ G. R. Bonneaud,²⁴ E. Latour,²⁴ M. Verderi,²⁴ P. J. Clark,²⁵ S. Playfer,²⁵ J. E. Watson,²⁵ M. Andreotti,^{26a,26b} D. Bettoni,^{26a} C. Bozzi,^{26a} R. Calabrese,^{26a,26b} A. Cecchi,^{26a,26b} G. Cibinetto,^{26a,26b} P. Franchini,^{26a,26b} E. Luppi,^{26a,26b} M. Negrini,^{26a,26b} A. Petrella,^{26a,26b} L. Piemontese,^{26a} V. Santoro,^{26a,26b} R. Baldini-Ferroli,²⁷ A. Calcaterra,²⁷ R. de Sangro,²⁷ G. Finocchiaro,²⁷ S. Pacetti,²⁷ P. Patteri,²⁷ I. M. Peruzzi,^{27,§} M. Piccolo,²⁷ M. Rama,²⁷ A. Zallo,²⁷ A. Buzzo,^{28a} R. Contri,^{28a,28b} M. Lo Vetere,^{28a,28b} M. M. Macri,^{28a} M. R. Monge,^{28a,28b} S. Passaggio,^{28a} C. Patrignani,^{28a,28b} E. Robutti,^{28a} A. Santroni,^{28a,28b} S. Tosi,^{28a,28b} K. S. Chaisanguanthum,²⁹ M. Morii,²⁹ A. Adametz,³⁰ J. Marks,³⁰ S. Schenk,³⁰ U. Uwer,³⁰ V. Klose,³¹ H. M. Lacker,³¹ D. J. Bard,³² P. D. Dauncey,³² J. A. Nash,³² M. Tibbetts,³² P. K. Behera,³³ X. Chai,³³ M. J. Charles,³³ U. Mallik,³³ J. Cochran,³⁴ H. B. Crawley,³⁴ L. Dong,³⁴ W. T. Meyer,³⁴ S. Prell,³⁴ E. I. Rosenberg,³⁴ A. E. Rubin,³⁴ Y. Y. Gao,³⁵ A. V. Gritsan,³⁵ Z. J. Guo,³⁵ C. K. Lae,³⁵ N. Arnaud,³⁶ J. Béguilleux,³⁶ A. D'Orazio,³⁶ M. Davier,³⁶ J. Firmino da Costa,³⁶ G. Grosdidier,³⁶ A. Höcker,³⁶ V. Lepeltier,³⁶ F. Le Diberder,³⁶ A. M. Lutz,³⁶ S. Pruvot,³⁶ P. Roudeau,³⁶ M. H. Schune,³⁶ J. Serrano,³⁶ V. Sordini,^{36,||} A. Stocchi,³⁶ G. Wormser,³⁶ D. J. Lange,³⁷ D. M. Wright,³⁷ I. Bingham,³⁸ J. P. Burke,³⁸ C. A. Chavez,³⁸ J. R. Fry,³⁸ E. Gabathuler,³⁸ R. Gamet,³⁸ D. E. Hutchcroft,³⁸ D. J. Payne,³⁸ C. Touramanis,³⁸ A. J. Bevan,³⁹ C. K. Clarke,³⁹ K. A. George,³⁹ F. Di Lodovico,³⁹ R. Sacco,³⁹ M. Sigamani,³⁹ G. Cowan,⁴⁰ H. U. Flaecher,⁴⁰ D. A. Hopkins,⁴⁰ S. Paramesvaran,⁴⁰ F. Salvatore,⁴⁰ A. C. Wren,⁴⁰ D. N. Brown,⁴¹ C. L. Davis,⁴¹ A. G. Denig,⁴² M. Fritsch,⁴² W. Gradl,⁴² G. Schott,⁴² K. E. Alwyn,⁴³ D. Bailey,⁴³ R. J. Barlow,⁴³ Y. M. Chia,⁴³ C. L. Edgar,⁴³ G. Jackson,⁴³ G. D. Lafferty,⁴³ T. J. West,⁴³ J. I. Yi,⁴³ J. Anderson,⁴⁴ C. Chen,⁴⁴ A. Jawahery,⁴⁴ D. A. Roberts,⁴⁴ G. Simi,⁴⁴ J. M. Tuggle,⁴⁴ C. Dallapiccola,⁴⁵ X. Li,⁴⁵ E. Salvati,⁴⁵ S. Saremi,⁴⁵ R. Cowan,⁴⁶ D. Dujmic,⁴⁶ P. H. Fisher,⁴⁶ G. Sciolla,⁴⁶ M. Spitznagel,⁴⁶ F. Taylor,⁴⁶ R. K. Yamamoto,⁴⁶ M. Zhao,⁴⁶ P. M. Patel,⁴⁷ S. H. Robertson,⁴⁷ A. Lazzaro,^{48a,48b} V. Lombardo,^{48a} F. Palombo,^{48a,48b} J. M. Bauer,⁴⁹ L. Cremaldi,⁴⁹ R. Godang,^{49,¶} R. Kroeger,⁴⁹ D. A. Sanders,⁴⁹ D. J. Summers,⁴⁹ H. W. Zhao,⁴⁹ M. Simard,⁵⁰ P. Taras,⁵⁰ F. B. Viaud,⁵⁰ H. Nicholson,⁵¹ G. De Nardo,^{52a,52b} L. Lista,^{52a} D. Monorchio,^{52a,52b} G. Onorato,^{52a,52b} C. Sciacca,^{52a,52b} G. Raven,⁵³ H. L. Snoek,⁵³ C. P. Jessop,⁵⁴ K. J. Knoepfel,⁵⁴ J. M. LoSecco,⁵⁴ W. F. Wang,⁵⁴ G. Benelli,⁵⁵ L. A. Corwin,⁵⁵ K. Honscheid,⁵⁵ H. Kagan,⁵⁵ R. Kass,⁵⁵ J. P. Morris,⁵⁵ A. M. Rahimi,⁵⁵ J. J. Regensburger,⁵⁵ S. J. Sekula,⁵⁵ Q. K. Wong,⁵⁵ N. L. Blount,⁵⁶ J. Brau,⁵⁶ R. Frey,⁵⁶ O. Igonkina,⁵⁶ J. A. Kolb,⁵⁶ M. Lu,⁵⁶ R. Rahmat,⁵⁶ N. B. Sinev,⁵⁶ D. Strom,⁵⁶ J. Strube,⁵⁶ E. Torrence,⁵⁶ G. Castelli,^{57a,57b} N. Gagliardi,^{57a,57b} M. Margoni,^{57a,57b} M. Morandin,^{57a} M. Posocco,^{57a} M. Rotondo,^{57a} F. Simonetto,^{57a,57b} R. Stroili,^{57a,57b} C. Voci,^{57a,57b} P. del Amo Sanchez,⁵⁸ E. Ben-Haim,⁵⁸ H. Briand,⁵⁸ G. Calderini,⁵⁸ J. Chauveau,⁵⁸ P. David,⁵⁸ L. Del Buono,⁵⁸ O. Hamon,⁵⁸ Ph. Leruste,⁵⁸ J. Ocariz,⁵⁸ A. Perez,⁵⁸ J. Prendki,⁵⁸ S. Sitt,⁵⁸ L. Gladney,⁵⁹ M. Biasini,^{60a,60b} R. Covarelli,^{60a,60b} E. Manoni,^{60a,60b} C. Angelini,^{61a,61b} G. Batignani,^{61a,61b} S. Bettarini,^{61a,61b} M. Carpinelli,^{61a,61b,**} A. Cervelli,^{61a,61b} F. Forti,^{61a,61b} M. A. Giorgi,^{61a,61b} A. Lusiani,^{61a,61c} G. Marchiori,^{61a,61b} M. Morganti,^{61a,61b} N. Neri,^{61a,61b} E. Paoloni,^{61a,61b} G. Rizzo,^{61a,61b} J. J. Walsh,^{61a} D. Lopes Pegna,⁶² C. Lu,⁶² J. Olsen,⁶² A. J. S. Smith,⁶² A. V. Telnov,⁶² F. Anulli,^{63a} E. Baracchini,^{63a,63b} G. Cavoto,^{63a} D. del Re,^{63a,63b} E. Di Marco,^{63a,63b} R. Faccini,^{63a,63b} F. Ferrarotto,^{63a} F. Ferroni,^{63a,63b} M. Gaspero,^{63a,63b} P. D. Jackson,^{63a} L. Li Gioi,^{63a} M. A. Mazzoni,^{63a} S. Morganti,^{63a}

G. Piredda,^{63a} F. Polci,^{63a,63b} F. Renga,^{63a,63b} C. Voena,^{63a} M. Ebert,⁶⁴ T. Hartmann,⁶⁴ H. Schröder,⁶⁴ R. Waldi,⁶⁴ T. Adye,⁶⁵ B. Franek,⁶⁵ E. O. Olaiya,⁶⁵ F. F. Wilson,⁶⁵ S. Emery,⁶⁶ M. Escalier,⁶⁶ L. Esteve,⁶⁶ S. F. Ganzhur,⁶⁶ G. Hamel de Monchenault,⁶⁶ W. Kozanecki,⁶⁶ G. Vasseur,⁶⁶ Ch. Yèche,⁶⁶ M. Zito,⁶⁶ X. R. Chen,⁶⁷ H. Liu,⁶⁷ W. Park,⁶⁷ M. V. Purohit,⁶⁷ R. M. White,⁶⁷ J. R. Wilson,⁶⁷ M. T. Allen,⁶⁸ D. Aston,⁶⁸ R. Bartoldus,⁶⁸ P. Bechtle,⁶⁸ J. F. Benitez,⁶⁸ R. Cenci,⁶⁸ J. P. Coleman,⁶⁸ M. R. Convery,⁶⁸ J. C. Dingfelder,⁶⁸ J. Dorfan,⁶⁸ G. P. Dubois-Felsmann,⁶⁸ W. Dunwoodie,⁶⁸ R. C. Field,⁶⁸ A. M. Gabareen,⁶⁸ S. J. Gowdy,⁶⁸ M. T. Graham,⁶⁸ P. Grenier,⁶⁸ C. Hast,⁶⁸ W. R. Innes,⁶⁸ J. Kaminski,⁶⁸ M. H. Kelsey,⁶⁸ H. Kim,⁶⁸ P. Kim,⁶⁸ M. L. Kocian,⁶⁸ D. W. G. S. Leith,⁶⁸ S. Li,⁶⁸ B. Lindquist,⁶⁸ S. Luitz,⁶⁸ V. Luth,⁶⁸ H. L. Lynch,⁶⁸ D. B. MacFarlane,⁶⁸ H. Marsiske,⁶⁸ R. Messner,⁶⁸ D. R. Muller,⁶⁸ H. Neal,⁶⁸ S. Nelson,⁶⁸ C. P. O'Grady,⁶⁸ I. Ofte,⁶⁸ A. Perazzo,⁶⁸ M. Perl,⁶⁸ B. N. Ratcliff,⁶⁸ A. Roodman,⁶⁸ A. A. Salnikov,⁶⁸ R. H. Schindler,⁶⁸ J. Schwiening,⁶⁸ A. Snyder,⁶⁸ D. Su,⁶⁸ M. K. Sullivan,⁶⁸ K. Suzuki,⁶⁸ S. K. Swain,⁶⁸ J. M. Thompson,⁶⁸ J. Va'vra,⁶⁸ A. P. Wagner,⁶⁸ M. Weaver,⁶⁸ C. A. West,⁶⁸ W. J. Wisniewski,⁶⁸ M. Wittgen,⁶⁸ D. H. Wright,⁶⁸ H. W. Wulsin,⁶⁸ A. K. Yarritu,⁶⁸ K. Yi,⁶⁸ C. C. Young,⁶⁸ V. Ziegler,⁶⁸ P. R. Burchat,⁶⁹ A. J. Edwards,⁶⁹ S. A. Majewski,⁶⁹ T. S. Miyashita,⁶⁹ B. A. Petersen,⁶⁹ L. Wilden,⁶⁹ S. Ahmed,⁷⁰ M. S. Alam,⁷⁰ J. A. Ernst,⁷⁰ B. Pan,⁷⁰ M. A. Saeed,⁷⁰ S. B. Zain,⁷⁰ S. M. Spanier,⁷¹ B. J. Wogland,⁷¹ R. Eckmann,⁷² J. L. Ritchie,⁷² A. M. Ruland,⁷² C. J. Schilling,⁷² R. F. Schwitters,⁷² B. W. Drummond,⁷³ J. M. Izen,⁷³ X. C. Lou,⁷³ F. Bianchi,^{74a,74b} D. Gamba,^{74a,74b} M. Pelliccioni,^{74a,74b} M. Bomben,^{75a,75b} L. Bosio,^{75a,75b} C. Cartaro,^{75a,75b} G. Della Ricca,^{75a,75b} L. Lanceri,^{75a,75b} L. Vitale,^{75a,75b} V. Azzolini,⁷⁶ N. Lopez-March,⁷⁶ F. Martinez-Vidal,⁷⁶ D. A. Milanes,⁷⁶ A. Oyanguren,⁷⁶ J. Albert,⁷⁷ Sw. Banerjee,⁷⁷ B. Bhuyan,⁷⁷ H. H. F. Choi,⁷⁷ K. Hamano,⁷⁷ R. Kowalewski,⁷⁷ M. J. Lewczuk,⁷⁷ I. M. Nugent,⁷⁷ J. M. Roney,⁷⁷ R. J. Sobie,⁷⁷ T. J. Gershon,⁷⁸ P. F. Harrison,⁷⁸ J. Ilic,⁷⁸ T. E. Latham,⁷⁸ G. B. Mohanty,⁷⁸ H. R. Band,⁷⁹ X. Chen,⁷⁹ S. Dasu,⁷⁹ K. T. Flood,⁷⁹ Y. Pan,⁷⁹ M. Pierini,⁷⁹ R. Prepost,⁷⁹ C. O. Vuosalo,⁷⁹ and S. L. Wu⁷⁹

(The *BABAR* Collaboration)

¹Laboratoire de Physique des Particules, IN2P3/CNRS et Université de Savoie, F-74941 Annecy-Le-Vieux, France

²Universitat de Barcelona, Facultat de Física, Departament ECM, E-08028 Barcelona, Spain

^{3a}INFN Sezione di Bari, I-70126 Bari, Italy

^{3b}Dipartimento di Fisica, Università di Bari, I-70126 Bari, Italy

⁴University of Bergen, Institute of Physics, N-5007 Bergen, Norway

⁵Lawrence Berkeley National Laboratory and University of California, Berkeley, California 94720, USA

⁶University of Birmingham, Birmingham, B15 2TT, United Kingdom

⁷Ruhr Universität Bochum, Institut für Experimentalphysik I, D-44780 Bochum, Germany

⁸University of Bristol, Bristol BS8 1TL, United Kingdom

⁹University of British Columbia, Vancouver, British Columbia, Canada V6T 1Z1

¹⁰Brunel University, Uxbridge, Middlesex UB8 3PH, United Kingdom

¹¹Budker Institute of Nuclear Physics, Novosibirsk 630090, Russia

¹²University of California at Irvine, Irvine, California 92697, USA

¹³University of California at Los Angeles, Los Angeles, California 90024, USA

¹⁴University of California at Riverside, Riverside, California 92521, USA

¹⁵University of California at San Diego, La Jolla, California 92093, USA

¹⁶University of California at Santa Barbara, Santa Barbara, California 93106, USA

¹⁷University of California at Santa Cruz, Institute for Particle Physics, Santa Cruz, California 95064, USA

¹⁸California Institute of Technology, Pasadena, California 91125, USA

¹⁹University of Cincinnati, Cincinnati, Ohio 45221, USA

²⁰University of Colorado, Boulder, Colorado 80309, USA

²¹Colorado State University, Fort Collins, Colorado 80523, USA

²²Technische Universität Dortmund, Fakultät Physik, D-44221 Dortmund, Germany

²³Technische Universität Dresden, Institut für Kern- und Teilchenphysik, D-01062 Dresden, Germany

²⁴Laboratoire Leprince-Ringuet, CNRS/IN2P3, Ecole Polytechnique, F-91128 Palaiseau, France

²⁵University of Edinburgh, Edinburgh EH9 3JZ, United Kingdom

^{26a}INFN Sezione di Ferrara, I-44100 Ferrara, Italy

^{26b}Dipartimento di Fisica, Università di Ferrara, I-44100 Ferrara, Italy

²⁷INFN Laboratori Nazionali di Frascati, I-00044 Frascati, Italy

^{28a}INFN Sezione di Genova, I-16146 Genova, Italy

^{28b}Dipartimento di Fisica, Università di Genova, I-16146 Genova, Italy

²⁹Harvard University, Cambridge, Massachusetts 02138, USA

³⁰Universität Heidelberg, Physikalisches Institut, Philosophenweg 12, D-69120 Heidelberg, Germany

- ³¹*Humboldt-Universität zu Berlin, Institut für Physik, Newtonstr. 15, D-12489 Berlin, Germany*
- ³²*Imperial College London, London, SW7 2AZ, United Kingdom*
- ³³*University of Iowa, Iowa City, Iowa 52242, USA*
- ³⁴*Iowa State University, Ames, Iowa 50011-3160, USA*
- ³⁵*Johns Hopkins University, Baltimore, Maryland 21218, USA*
- ³⁶*Laboratoire de l'Accélérateur Linéaire, IN2P3/CNRS et Université Paris-Sud 11, Centre Scientifique d'Orsay, B. P. 34, F-91898 Orsay Cedex, France*
- ³⁷*Lawrence Livermore National Laboratory, Livermore, California 94550, USA*
- ³⁸*University of Liverpool, Liverpool L69 7ZE, United Kingdom*
- ³⁹*Queen Mary, University of London, London, E1 4NS, United Kingdom*
- ⁴⁰*University of London, Royal Holloway and Bedford New College, Egham, Surrey TW20 0EX, United Kingdom*
- ⁴¹*University of Louisville, Louisville, Kentucky 40292, USA*
- ⁴²*Johannes Gutenberg-Universität Mainz, Institut für Kernphysik, D-55099 Mainz, Germany*
- ⁴³*University of Manchester, Manchester M13 9PL, United Kingdom*
- ⁴⁴*University of Maryland, College Park, Maryland 20742, USA*
- ⁴⁵*University of Massachusetts, Amherst, Massachusetts 01003, USA*
- ⁴⁶*Massachusetts Institute of Technology, Laboratory for Nuclear Science, Cambridge, Massachusetts 02139, USA*
- ⁴⁷*McGill University, Montréal, Québec, Canada H3A 2T8*
- ^{48a}*INFN Sezione di Milano, I-20133 Milano, Italy*
- ^{48b}*Dipartimento di Fisica, Università di Milano, I-20133 Milano, Italy*
- ⁴⁹*University of Mississippi, University, Mississippi 38677, USA*
- ⁵⁰*Université de Montréal, Physique des Particules, Montréal, Québec, Canada H3C 3J7*
- ⁵¹*Mount Holyoke College, South Hadley, Massachusetts 01075, USA*
- ^{52a}*INFN Sezione di Napoli, I-80126 Napoli, Italy*
- ^{52b}*Dipartimento di Scienze Fisiche, Università di Napoli Federico II, I-80126 Napoli, Italy*
- ⁵³*NIKHEF, National Institute for Nuclear Physics and High Energy Physics, NL-1009 DB Amsterdam, The Netherlands*
- ⁵⁴*University of Notre Dame, Notre Dame, Indiana 46556, USA*
- ⁵⁵*Ohio State University, Columbus, Ohio 43210, USA*
- ⁵⁶*University of Oregon, Eugene, Oregon 97403, USA*
- ^{57a}*INFN Sezione di Padova, I-35131 Padova, Italy*
- ^{57b}*Dipartimento di Fisica, Università di Padova, I-35131 Padova, Italy*
- ⁵⁸*Laboratoire de Physique Nucléaire et de Hautes Energies, IN2P3/CNRS, Université Pierre et Marie Curie-Paris6, Université Denis Diderot-Paris7, F-75252 Paris, France*
- ⁵⁹*University of Pennsylvania, Philadelphia, Pennsylvania 19104, USA*
- ^{60a}*INFN Sezione di Perugia, I-06100 Perugia, Italy*
- ^{60b}*Dipartimento di Fisica, Università di Perugia, I-06100 Perugia, Italy*
- ^{61a}*INFN Sezione di Pisa, I-56127 Pisa, Italy*
- ^{61b}*Dipartimento di Fisica, Università di Pisa, I-56127 Pisa, Italy*
- ^{61c}*Scuola Normale Superiore di Pisa, I-56127 Pisa, Italy*
- ⁶²*Princeton University, Princeton, New Jersey 08544, USA*
- ^{63a}*INFN Sezione di Roma, I-00185 Roma, Italy*
- ^{63b}*Dipartimento di Fisica, Università di Roma La Sapienza, I-00185 Roma, Italy*
- ⁶⁴*Universität Rostock, D-18051 Rostock, Germany*
- ⁶⁵*Rutherford Appleton Laboratory, Chilton, Didcot, Oxon, OX11 0QX, United Kingdom*
- ⁶⁶*CEA, Irfu, SPP, Centre de Saclay, F-91191 Gif-sur-Yvette, France*
- ⁶⁷*University of South Carolina, Columbia, South Carolina 29208, USA*
- ⁶⁸*Stanford Linear Accelerator Center, Stanford, California 94309, USA*
- ⁶⁹*Stanford University, Stanford, California 94305-4060, USA*
- ⁷⁰*State University of New York, Albany, New York 12222, USA*
- ⁷¹*University of Tennessee, Knoxville, Tennessee 37996, USA*
- ⁷²*University of Texas at Austin, Austin, Texas 78712, USA*
- ⁷³*University of Texas at Dallas, Richardson, Texas 75083, USA*

*Deceased

+Now at Temple University, Philadelphia, PA 19122, USA

‡Now at Tel Aviv University, Tel Aviv, 69978, Israel

§Also with Università di Perugia, Dipartimento di Fisica, Perugia, Italy

||Also with Università di Roma La Sapienza, I-00185 Roma, Italy

¶Now at University of South Alabama, Mobile, AL 36688, USA

**Also with Università di Sassari, Sassari, Italy

^{74a}*INFN Sezione di Torino, I-10125 Torino, Italy*^{74b}*Dipartimento di Fisica Sperimentale, Università di Torino, I-10125 Torino, Italy*^{75a}*INFN Sezione di Trieste, I-34127 Trieste, Italy*^{75b}*Dipartimento di Fisica, Università di Trieste, I-34127 Trieste, Italy*⁷⁶*IFIC, Universitat de Valencia-CSIC, E-46071 Valencia, Spain*⁷⁷*University of Victoria, Victoria, British Columbia, Canada V8W 3P6*⁷⁸*Department of Physics, University of Warwick, Coventry CV4 7AL, United Kingdom*⁷⁹*University of Wisconsin, Madison, Wisconsin 53706, USA*

(Received 11 August 2008; published 6 November 2008)

We present the observation of the decay $B^0 \rightarrow \chi_{c0} K^{*0}$ as well as evidence of $B^+ \rightarrow \chi_{c0} K^{*+}$, with an 8.9 and a 3.6 standard deviation significance, respectively, using a data sample of 454×10^6 $Y(4S) \rightarrow B\bar{B}$ decays collected with the *BABAR* detector at the PEP-II B meson factory located at the Stanford Linear Accelerator Center (SLAC). The measured branching fractions are $\mathcal{B}(B^0 \rightarrow \chi_{c0} K^{*0}) = (1.7 \pm 0.3 \pm 0.2) \times 10^{-4}$ and $\mathcal{B}(B^+ \rightarrow \chi_{c0} K^{*+}) = (1.4 \pm 0.5 \pm 0.2) \times 10^{-4}$, where the first quoted errors are statistical and the second are systematic. We obtain a branching fraction upper limit of $\mathcal{B}(B^+ \rightarrow \chi_{c0} K^{*+}) < 2.1 \times 10^{-4}$ at the 90% confidence level.

DOI: 10.1103/PhysRevD.78.091101

PACS numbers: 13.25.Hw

Theoretical predictions of branching fractions and rate asymmetries in nonleptonic heavy-flavor meson decays are difficult due to our limited understanding of the process of quark hadronization. In the simplest approximation, weak decays such as $B \rightarrow J/\psi K$ arise from the quark-level process $b \rightarrow c\bar{c}s$ through a current-current interaction that can be written as $[\bar{c}\gamma^\mu(1-\gamma_5)c][\bar{s}\gamma_\mu(1-\gamma_5)b]$, where γ_μ are Dirac matrices ($\mu = 0, 1, 2, 3$), $\gamma_5 = \gamma_0\gamma_1\gamma_2\gamma_3$ and \bar{c}, c, \bar{s}, b are quark spinor fields. The colorless current $\bar{c}\gamma^\mu(1-\gamma_5)c$, which can create the J/ψ , can also create the P -wave state χ_{c1} . It cannot, however, create the χ_{c0}, χ_{c2} or h_c states, so their appearance would have to be explained by a more complex hypothesis. A theoretical prediction can be obtained with the factorization hypothesis [1], assuming that the weak decay matrix element can be described as a product of two independent hadronic currents. Under the factorization hypothesis, $B \rightarrow c\bar{c}K^{(*)}$ decays are allowed when the $c\bar{c}$ pair hadronizes to $J/\psi, \psi(2S)$ or χ_{c1} , but suppressed when the $c\bar{c}$ pair hadronizes to χ_{c0} [2]. In lowest-order Heavy Quark Effective Theory, the decay rate to the scalar χ_{c0} is zero due to charge conjugation invariance [3].

The decay $B^+ \rightarrow \chi_{c0} K^+$ has been observed by Belle and *BABAR* with an average branching fraction (\mathcal{B}) of $(1.40_{-0.19}^{+0.23}) \times 10^{-4}$ [4], using χ_{c0} decays to $K^+ K^-$ or $\pi^+ \pi^-$. This result is of the same order of magnitude as the branching fraction of the decay $B^+ \rightarrow \chi_{c1} K^+$, $(4.9 \pm 0.5) \times 10^{-4}$ [4], and is surprisingly large given the expectation from factorization. Using the hadronic χ_{c0} decays, Belle has obtained an upper limit on $B^0 \rightarrow \chi_{c0} K^0$ of 1.1×10^{-4} at 90% confidence level [5]. No predictions are available for B decays to $\chi_{c0} K^*$, so the branching fraction measurement of $B \rightarrow \chi_{c0} K^*$ should improve our understanding of the limitations of factorization and of models that do not rely on factorization.

In this paper we report the first observation of $B^0 \rightarrow \chi_{c0} K^{*0}$ and find evidence of the decay $B^+ \rightarrow \chi_{c0} K^{*+}$ [6].

We identify χ_{c0} mesons through their decays to $h^+ h^-$ ($h = K, \pi$), as $\chi_{c0} \rightarrow K^+ K^-$ and $\chi_{c0} \rightarrow \pi^+ \pi^-$ have a higher branching fraction than the radiative decay to $J/\psi \gamma$ ($J/\psi \rightarrow l^+ l^-, l = \mu$ or e), that was used in the previous search for $B \rightarrow \chi_{c0} K^*$ [7]. We identify K^{*+} mesons through their decay to $K_S^0 \pi^+$, where $K_S^0 \rightarrow \pi^+ \pi^-$, and K^{*0} mesons through their decay to $K^+ \pi^-$.

The data on which this analysis is based were collected with the *BABAR* detector [8] at the PEP-II asymmetric-energy $e^+ e^-$ storage ring. The *BABAR* detector consists of a double-sided five-layer silicon tracker, a 40-layer drift chamber, a Cherenkov detector, an electromagnetic calorimeter, and a magnet with instrumented flux return (IFR) consisting of layers of iron interspersed with resistive plate chambers and limited streamer tubes. The data sample has an integrated luminosity of 413 fb^{-1} collected at the $Y(4S)$ resonance, which corresponds to $(454 \pm 5) \times 10^6$ $B\bar{B}$ pairs. It is assumed that the $Y(4S)$ decays equally to neutral and charged B meson pairs. In addition, 41 fb^{-1} of data collected 40 MeV below the $Y(4S)$ resonance (off-resonance data) are used for background studies.

Candidate B mesons are reconstructed from five tracks for charged B decays and four tracks for neutral B decays, where three and four tracks, respectively, are consistent with originating from a common decay point within the PEP-II luminous region. Each of the tracks is required to have a transverse momentum greater than 50 MeV/ c and an absolute momentum less than 10 GeV/ c . The tracks are identified as either pion or kaon candidates, with protons vetoed, using Cherenkov-angle information and ionization energy-loss rate (dE/dx) measurements. The efficiency for kaon selection is approximately 80%, including geometric acceptance, while the probability of misidentification of pions as kaons is below 5% up to a laboratory momentum of 4 GeV/ c . Muons are rejected using information predominantly from the IFR. Furthermore, the tracks are required to fail an electron selection based on their ratio

of energy deposited in the calorimeter to momentum measured in the drift chamber, shower shape in the calorimeter, dE/dx , and Cherenkov-angle information. Candidate K_S^0 mesons are reconstructed from $\pi^+ \pi^-$ candidates, and are required to have a reconstructed mass within $15 \text{ MeV}/c^2$ of the nominal K^0 mass [4], a decay vertex separated from the B^+ decay vertex with a significance of at least 5 standard deviations, a flight distance in the transverse direction of at least 0.3 cm and a cosine of the angle between the line joining the B and K_S^0 decay vertices and the K_S^0 momentum greater than 0.999.

Four kinematic variables and one event-shape variable are used to characterize signal events. The first kinematic variable, ΔE , is the difference between the center-of-mass (c.m.) energy of the B candidate and $\sqrt{s}/2$, where \sqrt{s} is the total c.m. energy. The second is the beam-energy-substituted mass $m_{\text{ES}} = \sqrt{(s/2 + \mathbf{p}_i \cdot \mathbf{p}_B)^2/E_i^2 - \mathbf{p}_B^2}$, where \mathbf{p}_B is the reconstructed momentum of the B candidate, and the four-momentum of its parent $Y(4S)$ in the laboratory frame, (E_i, \mathbf{p}_i) , is determined from nominal colliding beam parameters. The third kinematic variable is the $K\pi$ invariant mass, m_{K^*} , used to identify K^* candidates, where $K\pi$ is $K_S^0 \pi^+$ or $K^+ \pi^-$ for K^{*+} or K^{*0} candidates, respectively. The fourth kinematic variable is the $h^+ h^-$ invariant mass, m_{hh} , used to identify χ_{c0} candidates. Candidate B mesons are required to satisfy $|\Delta E| < 0.1 \text{ GeV}$, $5.25 < m_{\text{ES}} < 5.29 \text{ GeV}/c^2$, $0.772(0.776) < m_{K^*} < 0.992(0.996) \text{ GeV}/c^2$ for $B^+(B^0)$ candidates and $3.35 < m_{hh} < 3.50 \text{ GeV}/c^2$. The event-shape variable is a Fisher discriminant \mathcal{F} [9], constructed as a linear combination of the absolute value of the cosine of the angle between the B candidate momentum and the beam axis, the absolute value of the cosine of the angle between the thrust axis of the decay products of the B candidate and the beam axis, and the zeroth and second angular moments of energy flow about the thrust axis of the reconstructed B .

Continuum quark production ($e^+ e^- \rightarrow q\bar{q}$, where $q = u, d, s, c$) is the dominant source of background. It is suppressed using another event-shape variable, $|\cos\theta_T|$, which is the absolute value of the cosine of the angle θ_T between the thrust axis [10] of the selected B candidate and the thrust axis of the rest of the event. For continuum background, the distribution of $|\cos\theta_T|$ is strongly peaked towards 1 whereas the distribution is essentially flat for signal events. Therefore, the relative amount of continuum background is reduced by requiring $|\cos\theta_T| < 0.9$.

Backgrounds from other B meson decays are studied with Monte Carlo (MC) events, using at least 10^3 times the number of events expected in data for specific decay modes that are the possible sources of background for this analysis.

Potential charm contributions from $B \rightarrow D(\rightarrow K^* h^-) h^+$ events are removed by vetoing events with a reconstructed $K^* h^-$ invariant mass in the range $1.83 < m_{K^* h^-} < 1.91 \text{ GeV}/c^2$. To remove background from D^0 mesons, a

veto is applied to any $K\pi$ pair with an invariant mass in the range $1.83 < m_{K\pi} < 1.91 \text{ GeV}/c^2$ for each $B \rightarrow \chi_{c0}(\rightarrow h^+ h^-) K^*$ decay. Studies of MC events show that the largest remaining charmed backgrounds are $B^+ \rightarrow \bar{D}^0(\rightarrow K_S^0 \pi^+ \pi^-) \pi^+$ and $B^0 \rightarrow D^-(\rightarrow K^+ \pi^- \pi^-) \pi^+$, with 12% and 10% passing the veto, respectively. Surviving charmed events have a reconstructed D mass outside the veto range as a result of using a π or K candidate that is incorrectly selected from the other B decay in the event.

A fraction of signal events has more than one B candidate reconstructed. For those events, the candidate with the highest χ^2 probability of the fitted B decay vertex is selected. Studies of MC events show that less than 11% of events are reconstructed from the wrong candidate, where these incorrectly reconstructed events are modeled in the fit to data.

After applying all selection criteria, there are five main categories of background from B decays: two- and three-body decays proceeding via a D meson; nonresonant $B \rightarrow K^* h^+ h^-$ and $B \rightarrow K\pi \chi_{c0}$; combinatorial background from three unrelated particles ($K^* h^+ h^-$); two- or four-body B decays with an extra or missing particle and three-body decays with one or more particles misidentified. Along with selection efficiencies obtained from MC simulation, existing branching fractions for these modes [4,11] are used to estimate their background contributions that are included separately and fixed in fits to data. For the nonresonant backgrounds, where there is no branching fraction information, fits to sideband data ($0.996 < m_{K^*} < 1.53 \text{ GeV}/c^2$ and $3.2 < m_{hh} < 3.35 \text{ GeV}/c^2$) are performed to estimate the background contributions.

In order to extract the signal event yield for the channel under study, an unbinned extended maximum likelihood fit is used. The likelihood function for N events is

$$\mathcal{L} = \frac{1}{N!} \exp\left(-\sum_{i=1}^M n_i\right) \prod_{j=1}^N \left(\sum_{i=1}^M n_i P_i(\vec{\alpha}, \vec{x}_j)\right), \quad (1)$$

where $M = 3$ is the number of hypotheses (signal, continuum background, and B background), n_i is the number of events for each hypothesis determined by maximizing the likelihood function, and $P_i(\vec{\alpha}, \vec{x}_j)$ is a probability density function (PDF) with the parameters $\vec{\alpha}$ and variables $\vec{x} = (m_{\text{ES}}, \Delta E, \mathcal{F}, m_{K^*} \text{ and } m_{hh})$. The PDF is a product $P_i(\vec{\alpha}, \vec{x}) = P_i(\vec{\alpha}_{m_{\text{ES}}}, m_{\text{ES}}) \times P_i(\vec{\alpha}_{\Delta E}, \Delta E) \times P_i(\vec{\alpha}_{\mathcal{F}}, \mathcal{F}) \times P_i(\vec{\alpha}_{m_{K^*}}, m_{K^*}) \times P_i(\vec{\alpha}_{m_{hh}}, m_{hh})$. Studies of MC simulation show that correlations between these variables are small for the signal and continuum background hypotheses. However, for B background, correlations of a few percent are observed between m_{ES} and ΔE , which are taken into account by forming a 2-dimensional PDF for these variables.

The parameters for signal and B background PDFs are determined from MC simulation. All continuum back-

ground parameters are allowed to vary in the fit, in order to help reduce systematic effects from this dominant event type. Sideband data, defined to be in the region $0.1 < \Delta E < 0.3$ GeV and $5.25 < m_{ES} < 5.29$ GeV/ c^2 , as well as off-resonance data, are used to model the continuum background PDFs. For the m_{ES} PDFs, a Gaussian distribution is used for signal and a threshold function [12] for continuum background. For the ΔE PDFs, a sum of two Gaussian distributions with distinct means and widths is used for the signal and a first-order polynomial for the continuum background. A two-dimensional (m_{ES} , ΔE) histogram is used for B background. The signal, continuum and B background \mathcal{F} PDFs are described using a sum of two Gaussian distributions with distinct means and widths. For m_{K^*} PDFs, a sum of a relativistic Breit-Wigner function [4] and a first-order polynomial describes each of the signal, continuum, and B background distributions. Within the m_{K^*} fit range, there is also the possibility of B background contributions from nonresonant and higher K^* resonances; these contributions are modeled in the fit using the LASS parametrization [13,14]. The contribution from this background is estimated by extrapolating a $K\pi$ invariant mass projection fitted in a higher-mass region ($0.996 < m_{K^*} < 1.53$ GeV/ c^2) into the signal region. This estimated background is modeled in the final fit to the signal region and assumes there are no interference effects between the $K\pi$ background and the $K^*(892)$ signal. Finally, for m_{hh} PDFs, a sum of a relativistic Breit-Wigner function and a first-order polynomial is used to describe the signal and a first-order polynomial to describe the continuum and B background distributions. The non-resonant h^+h^- background is modeled by a first-order polynomial, and the background is estimated by extrapolating the invariant mass projection fitted in the lower mass region ($3.2 < m_{hh} < 3.35$ GeV/ c^2) into the signal region. The signal first-order polynomial component of the m_{K^*} and m_{hh} PDFs is used to model misreconstructed events; for example, where a K^+ from the K^{*0} is reconstructed as a χ_{c0} daughter particle, and vice versa.

To extract the $B \rightarrow \chi_{c0}K^*$ branching fractions, \mathcal{B} , the following equation is used:

$$\mathcal{B} = \frac{n_{\text{sig}}}{N_{BB} \times \epsilon \times \mathcal{B}(\chi_{c0} \rightarrow h^+h^-)}, \quad (2)$$

where n_{sig} is the number of signal events fitted, ϵ is the signal efficiency obtained from MC and N_{BB} is the total number of $B\bar{B}$ events. The efficiencies take into account both $\mathcal{B}(K^{*+} \rightarrow K^0\pi^+) = 2/3$ and $\mathcal{B}(K^{*0} \rightarrow K^+\pi^-) = 2/3$, assuming isospin symmetry, as well as $\mathcal{B}(K^0 \rightarrow K_S^0) = 1/2$ and $\mathcal{B}(K_S^0 \rightarrow \pi^+\pi^-)$ [4]. The branching fractions are calculated taking into account $\mathcal{B}(\chi_{c0} \rightarrow K^+K^-) = (5.5 \pm 0.6) \times 10^{-3}$ and $\mathcal{B}(\chi_{c0} \rightarrow \pi^+\pi^-) = (7.3 \pm 0.6) \times 10^{-3}$ [4].

We observe the decay $B^0 \rightarrow \chi_{c0}K^{*0}$ with an 8.9 standard deviation significance and measure the branching fraction

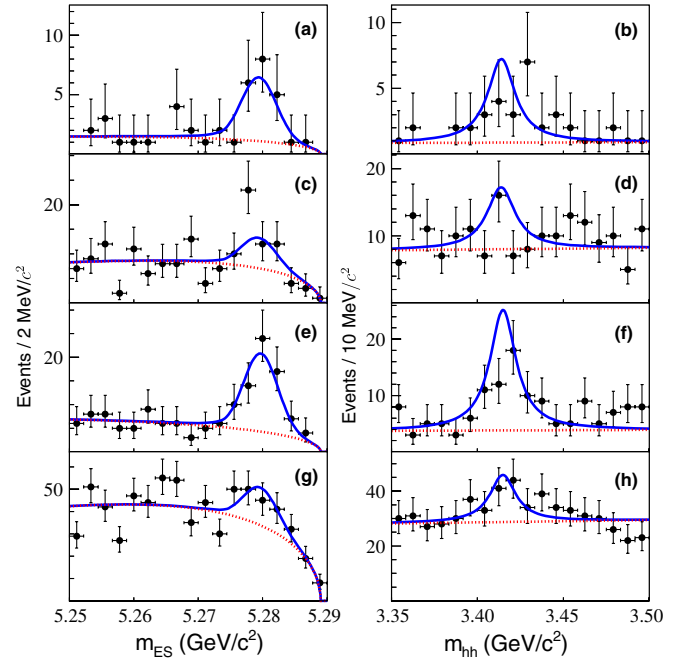


FIG. 1 (color online). Maximum likelihood fit projections of m_{ES} (left column) and m_{hh} (right column) for signal-enhanced samples of $B \rightarrow \chi_{c0}K^*$ candidates. The dashed line is the fitted background PDF while the solid line is the sum of the signal and background PDFs. The points indicate the data. The plot shows projections for $B^+ \rightarrow \chi_{c0}K^{*+}(\chi_{c0} \rightarrow K^+K^-)$ (a) and (b), for $B^+ \rightarrow \chi_{c0}K^{*+}(\chi_{c0} \rightarrow \pi^+\pi^-)$ (c) and (d), for $B^0 \rightarrow \chi_{c0}K^{*0}(\chi_{c0} \rightarrow K^+K^-)$ (e) and (f), and $B^0 \rightarrow \chi_{c0}K^{*0}(\chi_{c0} \rightarrow \pi^+\pi^-)$ (g) and (h).

$\mathcal{B}(B^0 \rightarrow \chi_{c0}K^{*0}) = (1.7 \pm 0.3 \pm 0.2) \times 10^{-4}$. We find evidence for $B^+ \rightarrow \chi_{c0}K^{*+}$ with a 3.6 standard deviation significance and set a 90% confidence level upper limit on the branching fraction of 2.1×10^{-4} . Figure 1 shows the fitted m_{ES} and m_{hh} projections for the $B^+ \rightarrow \chi_{c0}K^{*+}(\chi_{c0} \rightarrow K^+K^-)$, $B^+ \rightarrow \chi_{c0}K^{*+}(\chi_{c0} \rightarrow \pi^+\pi^-)$, $B^0 \rightarrow \chi_{c0}K^{*0}(\chi_{c0} \rightarrow K^+K^-)$ and $B^0 \rightarrow \chi_{c0}K^{*0}(\chi_{c0} \rightarrow \pi^+\pi^-)$ candidates, while the fitted signal yields; measured branching fractions and upper limits are shown in Table I. The candidates in Fig. 1 are signal-enhanced, with a requirement on the probability ratio $\mathcal{P}_{\text{sig}}/(\mathcal{P}_{\text{sig}} + \mathcal{P}_{\text{bkg}})$, optimized to enhance the visibility of potential signal, where \mathcal{P}_{sig} and \mathcal{P}_{bkg} are the signal and the total background probabilities, respectively (computed without using the variable plotted). Figure 2 shows the $-2 \ln \mathcal{L}$ distributions for both $B^+ \rightarrow \chi_{c0}K^{*+}$ and $B^0 \rightarrow \chi_{c0}K^{*0}$ as a function of the branching fraction. The $-2 \ln \mathcal{L}$ distributions for the final states ($\chi_{c0} \rightarrow K^+K^-$ and $\chi_{c0} \rightarrow \pi^+\pi^-$) are combined to give final the branching fractions shown in Table I. The 90% confidence level branching fraction upper limit (\mathcal{B}_{UL}) is determined by integrating the likelihood distribution (with systematic uncertainties included) as a function of the branching fraction from 0 to \mathcal{B}_{UL} , so that $\int_0^{\mathcal{B}_{\text{UL}}} \mathcal{L} d\mathcal{B} = 0.9 \int_0^\infty \mathcal{L} d\mathcal{B}$. The signal significance S , in

TABLE I. Total number of events in the fit, B background yields (B bkg), signal yields, efficiencies, and branching fractions \mathcal{B} , measured using $B \rightarrow \chi_{c0} K^{*}$ events. Fit bias corrections are applied to the signal yields and branching fractions. The first error is statistical and the second error is systematic. The significance S is shown for $B^+ \rightarrow \chi_{c0} K^{*+}$ and $B^0 \rightarrow \chi_{c0} K^{*0}$ and the branching fraction upper limit, \mathcal{B}_{UL} , at the 90% confidence level is shown for $B^+ \rightarrow \chi_{c0} K^{*+}$.

Mode	Total Events	B bkg	Signal Yield	Signal Efficiency (%)	$\mathcal{B} (\times 10^{-4})$	$\mathcal{B}_{\text{UL}} (\times 10^{-4})$	$S (\sigma)$
$B^+ \rightarrow \chi_{c0} K^{*+}$							
$\chi_{c0} \rightarrow K^+ K^-$	156	8	13 ± 5	3.2	$1.6 \pm 0.7 \pm 0.2$		
$\chi_{c0} \rightarrow \pi^+ \pi^-$	1065	65	15 ± 9	3.8	$1.2 \pm 0.7 \pm 0.2$		
Combined					$1.4 \pm 0.5 \pm 0.2$	2.1	3.6
$B^0 \rightarrow \chi_{c0} K^{*0}$							
$\chi_{c0} \rightarrow K^+ K^-$	690	20	47 ± 10	11.1	$1.7 \pm 0.4 \pm 0.2$		
$\chi_{c0} \rightarrow \pi^+ \pi^-$	4507	154	72 ± 15	12.8	$1.7 \pm 0.4 \pm 0.2$		
Combined					$1.7 \pm 0.3 \pm 0.2$		8.9

units of standard deviation, is defined as $\sqrt{2\Delta \ln \mathcal{L}}$, where $\Delta \ln \mathcal{L}$ represents the change in log-likelihood (with systematic uncertainties included) between the maximum value and the value when the signal yield is set to zero.

Contributions to the branching fraction systematic uncertainty are shown in Table II. The presence of a non-resonant $K^+ K^-$ and $\pi^+ \pi^-$ can give rise to interference effects, resulting in a departure from the m_{hh} PDF used in the fit to data. In order to estimate how much this can affect the extracted yields, the fit is repeated with the inclusion of

a PDF describing the interference between the Breit-Wigner and nonresonant amplitudes in the m_{hh} distribution. This shape consists of the squared modulus of the sum of a Breit-Wigner and a constant amplitude, carrying an arbitrary phase difference. The relative weight of these two components and their phase difference are allowed to vary to obtain the best fit. The signal yields derived from this fit are larger than the nominal fit in Table I, and the difference from the nominal fit is used as an estimate of the systematic error in Table II due to neglecting interference effects. Interference effects between the $K^*(892)$ and spin-0 final states (nonresonant and $K_0^*(1430)$) integrate to zero if the acceptance of the detector and analysis is uniform; the same is true of the interference between the $K^*(892)$ and

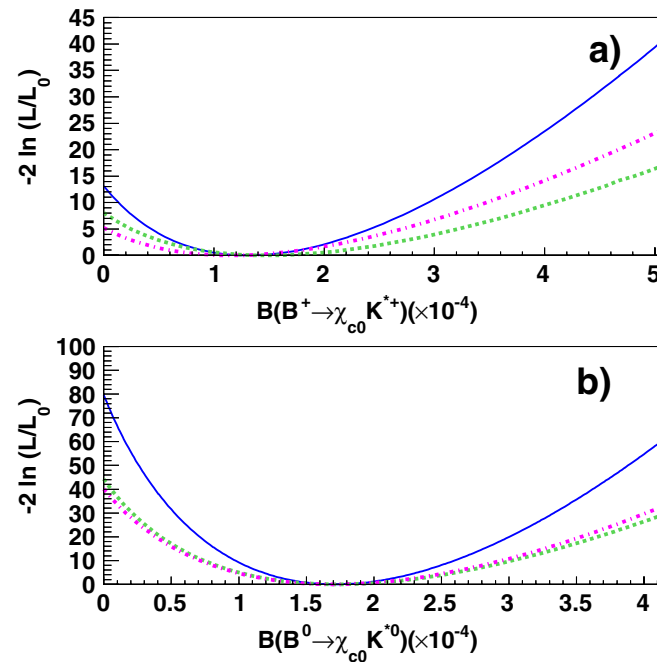


FIG. 2 (color online). Distribution of $-2 \ln \mathcal{L}$ as a function of branching fraction for $B^+ \rightarrow \chi_{c0} K^{*+}$ (a) and $B^0 \rightarrow \chi_{c0} K^{*0}$ (b). In each case, the upper dashed line is the decay $\chi_{c0} \rightarrow K^+ K^-$ and the lower dashed line is the decay $\chi_{c0} \rightarrow \pi^+ \pi^-$. The solid line is the combination of the two. In all cases systematics contributions are included and the $-2 \ln \mathcal{L}$ distributions have been shifted vertically so the minimum value is 0.

TABLE II. Summary of systematic uncertainty contributions to the branching fraction measurements $B \rightarrow \chi_{c0} K^{*}$. Multiplicative and additive errors are shown as a percentage of the branching fraction. The final row shows the total systematic error on the branching fractions.

Error Source	$\chi_{c0} K^{*+}$ $\chi_{c0}(KK)$	$\chi_{c0} K^{*+}$ $\chi_{c0}(\pi\pi)$	$\chi_{c0} K^{*0}$ $\chi_{c0}(KK)$	$\chi_{c0} K^{*0}$ $\chi_{c0}(\pi\pi)$
Multiplicative errors (%)				
Interference	7.2	8.3	6.8	10.1
Tracking	4.0	4.0	3.2	3.2
K_S^0 Efficiency	1.7	1.7	-	-
Particle ID	1.9	2.7	2.4	3.2
$\mathcal{B}(\chi_{c0} \rightarrow h^+ h^-)$	10.9	8.2	10.9	8.2
No. of $B\bar{B}$	1.1	1.1	1.1	1.1
Tot. mult. (%)	13.9	12.8	13.8	13.8
Additive errors (%)				
Fit Bias	1.3	4.4	1.8	3.9
B background	0.5	4.5	1.4	1.5
PDF params.	0.6	3.4	0.3	2.6
Tot. add. (%)	1.5	7.2	2.3	4.9
Total (10^{-4})	0.2	0.2	0.2	0.2

spin-2 final states ($K_2^*(1430)$). Studies of MC events show the efficiency variations are small enough to consider these interference effects insignificant. The integrated interference between $K^*(892)$ and other spin-1 amplitudes such as $K^*(1410)$ is in principle nonzero, but in practice is negligible due to the small branching fraction of $K^*(1410) \rightarrow K^+ \pi^-$ ($6.6 \pm 1.3\%$ [4]) and the fact that the $K\pi$ mass lineshapes have little overlap. Errors due to tracking efficiency, K_S^0 reconstruction efficiency and particle identification are assigned by comparing control channels in MC simulation and data. The branching fraction error of $\chi_{c0} \rightarrow h^+ h^-$ is taken from the combination of previous measurements [4]. The number of $B\bar{B}$ events is determined with an uncertainty of 1.1%. To estimate errors due to the fit procedure, 500 MC samples containing the numbers of signal and continuum events measured in data and the estimated number of exclusive B background events are used. The differences between the generated and fitted values are used to estimate small fit biases (see Table II) that are a consequence of correlations between fit variables. These biases are applied as corrections to obtain the final signal yields, and half of the correction is added as a systematic uncertainty. The uncertainty of the B background contribution to the fit is estimated by varying the known branching fractions within their errors. Each background is varied individually and the effect on the fitted signal yield is added in quadrature as a contribution to the uncertainty. The uncertainty due to PDF modeling is estimated by varying the PDFs by the parameter errors. In

order to take correlations between parameters into account, the full correlation matrix is used when varying the parameters. All PDF parameters that are originally fixed in the fit are then varied in turn, and each difference from the nominal fit is combined in quadrature and taken as a systematic contribution.

In summary, we have observed the decay $B^0 \rightarrow \chi_{c0} K^{*0}$ with an 8.9 standard deviation significance and find evidence for $B^+ \rightarrow \chi_{c0} K^{*+}$ with a 3.6 standard deviation significance, placing an upper limit on the branching fraction. The $B^0 \rightarrow \chi_{c0} K^{*0}$ branching fraction does not agree with the zero value expected from the color-singlet current-current contribution alone, and is approximately half the $B^0 \rightarrow \chi_{c1} K^{*0}$ branching fraction ($(3.2 \pm 0.6) \times 10^{-4}$ [4]), which is surprising when taking into account factorization expectations.

We are grateful for the excellent luminosity and machine conditions provided by our PEP-II colleagues, and for the substantial dedicated effort from the computing organizations that support *BABAR*. The collaborating institutions wish to thank SLAC for its support and kind hospitality. This work is supported by DOE and NSF (USA), NSERC (Canada), CEA and CNRS-IN2P3 (France), BMBF and DFG (Germany), INFN (Italy), FOM (The Netherlands), NFR (Norway), MIST (Russia), MEC (Spain), and STFC (United Kingdom). Individuals have received support from the Marie Curie EIF (European Union) and the A. P. Sloan Foundation.

-
- [1] M. Bauer, B. Stech, and M. Wirbel, *Z. Phys. C* **34**, 103 (1987).
 - [2] M. Suzuki, *Phys. Rev. D* **66**, 037503 (2002).
 - [3] M. Diehl and G. Hiller, *J. High Energy Phys.* **06** (2001) 067.
 - [4] W.M. Yao *et al.* (Particle Data Group), *J. Phys. G* **33**, 1 (2006), and 2007 partial update for the 2008 edition.
 - [5] A. Garmash *et al.* (Belle Collaboration), *Phys. Rev. D* **75**, 012006 (2007).
 - [6] The use of charge-conjugate modes is implied throughout this paper unless otherwise noted.
 - [7] B. Aubert *et al.* (*BABAR* Collaboration), *Phys. Rev. Lett.* **94**, 171801 (2005).
 - [8] B. Aubert *et al.* (*BABAR* Collaboration), *Nucl. Instrum. Methods Phys. Res., Sect. A* **479**, 1 (2002).
 - [9] R. A. Fisher, *Ann. Eugenics* **7**, 179 (1936); G. Cowan, *Statistical Data Analysis* (Oxford University Press, New York, 1998), Vol. 51.
 - [10] S. Brandt *et al.*, *Phys. Lett.* **12**, 57 (1964); E. Fahren, *Phys. Rev. Lett.* **39**, 1587 (1977).
 - [11] The Heavy Flavor Averaging Group (HFAG), <http://www.slac.stanford.edu/xorg/hfag/>.
 - [12] H. Albrecht *et al.* (ARGUS Collaboration), *Z. Phys. C* **48**, 543 (1990).
 - [13] D. Aston *et al.*, *Nucl. Phys.* **B296**, 493 (1988).
 - [14] B. Aubert *et al.* (*BABAR* Collaboration), *Phys. Rev. D* **72**, 072003 (2005).